Inorg. Chem. **2007**, *46*, 125–135

Modulation of the Singlet–Singlet Through-Space Energy Transfer Rates in Cofacial Bisporphyrin and Porphyrin–Corrole Dyads

Claude P. Gros,[†] Frédéric Brisach,[‡] Anastasia Meristoudi,[†] Enrique Espinosa,[†] Roger Guilard,*[,†] and Pierre D. Harvey*[,‡]

LIMSAG, Université de Bourgogne, 9 Avenue Alain Savary, BP 47870, 21078 Dijon Cedex France, and Département de Chimie, Université de Sherbrooke, Sherbrooke J1K 2R1, Québec, Canada

Received July 20, 2006

A new series of relatively flexible cofacial donor–acceptor dyads for singlet–singlet energy transfer with the corrole or *etio*-porphyrin free base and zinc porphyrin as the acceptor and donor, respectively, were synthesized and characterized (represented as $(PMes_2COx)ZnH_3$ (**13**), $(PMes_2CO)ZnH_3$ (**14**), and $(PMes_2CX)ZnH_3$ (**15**)) where ($PMes_2$-COx = [2-[5-(5,15-dimesitylcorrol-10-yl)-diphenylether-2′-yl]-13,17-diethyl-2,3,7,8,12,18-hexamethylporphyrin]), ($PMes_2$-CO = [5-[5-(5,15-dimesitylcorrol-10-yl)-dibenzofuran-4-yl]-13,17-diethyl-2,3,7,8,12,18-hexamethylporphyrin]), and ($PMes_2CX$ = [5-[5-(5,15-dimesitylcorrol-10-yl)-9,9-dimethylxanthen-4-yl)]-13,17-diethyl-2,3,7,8,12,18-hexamethylporphyrin]), respectively) along with the homobismacrocycles $(DPOx)ZnH_2$ (**17**) and $(DPOx)Zn_2$ (**18**) (where (DPOx = 2,2′-bis[5-(2,8,13,17-tetraethyl-3,7,12,18-tetramethylporphyrinyl)]diphenylether) as comparison standards. The rate for energy transfer (k_{ET}) extracted by the measurements of fluorescence lifetimes are of the same order of magnitude as those recently reported for the rigidly held face-to-face dyads ($(DPB)ZnH_2$ (**1**), $(DPX)ZnH_2$ (**2**), $(DPA)ZnH_2$ (**3**), $(DPO)ZnH_2$ (**4**), and $(DPS)ZnH_2$ (**5**) where (DPB = 1,8-bis[5-(2,8,13,17-tetraethyl-3,7,12,18-tetramethylporphyrinyl)]-biphenylene), (DPX = 4,5-bis[5-(2,8,13,17-tetraethyl-3,7,12,18-tetramethylporphyrinyl)]-9,9-dimethylxanthene), (DPA = 1,8-bis[5-(2,8,13,17-tetraethyl-3,7,12,18-tetramethylporphyrinyl)]anthracene), (DPO = 4,6-bis[5-(2,8,13,17-tetraethyl-3,7,12,18-tetramethylporphyrinyl)]dibenzofuran), and (DPS = 4,6-bis[5-(2,8,13,17-tetraethyl-3,7,12,18-tetramethylporphyrinyl)]dibenzothiophene), respectively), but for the first time, it is shown that the presence of a bulky group located between the acceptor and the donor moiety influences the transfer rate. The presence of perpendicular mesityl groups on the acceptor macrocycle prevents the two macrorings from interacting strongly; therefore, k_{ET} is slower. On the other hand, by rendering the rigid spacer flexible (i.e., changing the dibenzofuran rigid spacer to the flexible diphenylether assembling fragment), k_{ET} increases due to stronger intermacrocycle interactions. This study is complemented by DFT computations (B3LYP/3-21G*) as a molecular modeling tool where subtle structural features explain the changes in k_{ET}. During the course of this study, X-ray structures of **17** and **18** were investigated and exhibit a linear stacking of the bismacrocycles where intermolecular porphyrin–porphyrin interactions are observed ($d_{inter(Zn\cdots Zn)}$ = 4.66 and 4.57 Å, for **17** and **18**, respectively).

Introduction

The structure elucidation of light-harvesting devices (LH1, LH2, and LH3) in the purple bacteria[1−7] shined light on the mechanism of the crucial antenna effect that sustains life in these organisms. It has quickly been recognized that the rate or energy transfer and excitonic processes were particularly fast, approaching almost perfect efficiency.[8,9] The key feature for these biomolecular solar panels is the ring-formed 16 B

* To whom correspondence should be addressed. Tel : (+33) 03-80-39-61-11 (R.G.); (+1) 819-821-7092 (P.D.H.). Fax: (+33) 03-80-39-61-17 (R.G.); (+1) 819-821-8017 (P.D.H.). E-mail: Roger.Guilard@u-bourgogne.fr (R.G.); Pierre.Harvey@USherbrooke.ca (P.D.H.).

[†] Université de Bourgogne.

[‡] Université de Sherbrooke.

(1) Karrasch, S.; Bullough, P. A.; Ghosh, R. *EMBO J.* **1995**, *14*, 631.

(2) Koepke, J.; Hu, X.; Muenke, C.; Schulten, K.; Michel, H. *Structure* **1996**, *4*, 581.

(3) McDermott, G.; Prince, S. M.; Freer, A. A.; Hawthornthwaite-Lawless, A. M.; Papiz, M. Z.; Cogdell, R. J.; Isaacs, N. W. *Nature* **1995**, *374*, 517.

(4) McLuskey, K.; Prince, S. M.; Cogdell, R. J.; Isaacs, N. W. *Biochemistry* **2001**, *40*, 8783.

10.1021/ic0613558 CCC: $37.00
Published on Web 12/10/2006

Chart 1

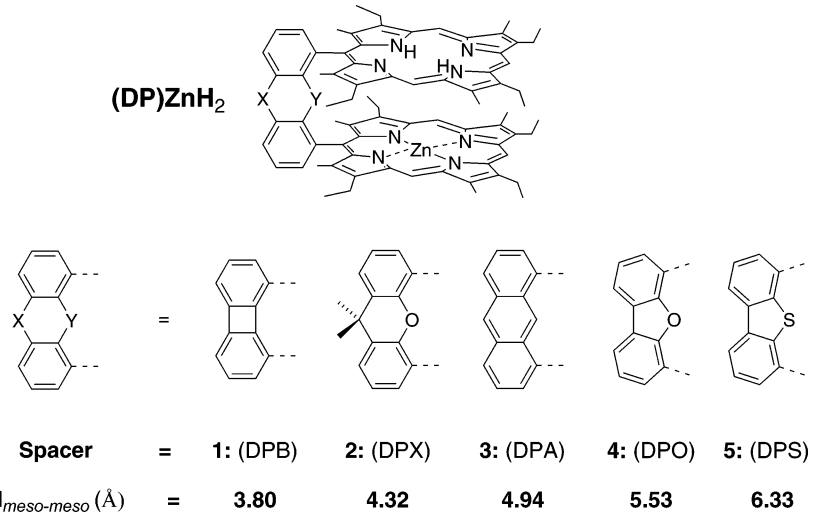

850 chlorophylls placed in a series of "slipped dimers" like J-aggregates, as recently well modeled by Takahashi and Kobuke.[10] The inter-chlorophyll metal-to-metal separation in the LH2 ring is about 8 Å. However, the closest distance between the π-carbons is shorter, suggesting that energy transport is more efficient at these locations.

In this respect, our research groups conducted a series of experiments on the role of the spacer on the rate of through space singlet−singlet energy transfer in rigidly held bisporphyrin systems placed face-to-face with $C_{meso}-C_{meso}$ varying from 3.8 to 6.3 Å (Chart 1).[11] The measured rates from the change in fluorescence lifetimes between Zn−porphyrin/free porphyrin donor−acceptor dyads and the corresponding homobimetallic donor−donor bismacrocycles increased as the distance $C_{meso}-C_{meso}$ decreased. Importantly, this work also estimated the critical distance where the switch in dominant mechanism is singlet−singlet energy transfer, Förster (electrostatic interactions)[12,13] vs Dexter (double electron transfer),[14] occurred (∼5 Å).[11] This distance was also confirmed for the triplet−triplet transfers where only one mechanism operates (Dexter).[15] Light harvesting devices in nature are multiple, and chlorophylls exist in different chemical versions (substituents), environment, and relative orientation despite similarities in chromophore−chromophore distances, responding to different biophysical and biochemical needs such as wavelength availability and amount of light.[16]

We now wish to report the modulation of the singlet−singlet through-space energy transfer in cofacial bisporphyrin and porphyrin−corrole dyads exhibiting very similar $C_{meso}-C_{meso}$ distances, but the relative orientation of the donor−acceptor pair is changed by the presence of bulky ligand and by the gain in flexibility of the spacer (Chart 2), hence changing the rate for transfer in a predictable manner (faster vs slower).

Experimental Section

Quantum Yields. All samples were prepared under inert atmosphere (in a glove box, $P_{O2} < 4-7$ ppm) by dissolution of the different compounds in 2-MeTHF using 1 cm^3 quartz cells with septum (298 K) or standard 5 mm NMR tubes (77 K). Three different measurements (i.e., different solutions) have been performed for each set of photophysical data (quantum yields and lifetimes). The sample concentrations were chosen to correspond to an absorbance of 0.05. Each absorbance value was measured five times for better accuracy in the measurements of the quantum yields. Reference for quantum yield was H_2TPP ($\Phi = 0.11$).[11,17]

Chemicals and Reagents. Absolute dichloromethane (CH_2Cl_2) was obtained from Fluka Chemical Co. and used as received. Neutral alumina (Merck; usually Brockmann Grade III, i.e., deactivated with 6% water) and silica gel (Merck; 70−120 mm) were used for column chromatography. Analytical thin layer chromatography was performed using Merck 60 F254 silica gel (precoated sheets, 0.2 mm thick). Reactions were monitored by thin-layer chromatography and UV−visible spectroscopy. Bis(2-formylphenyl)ether is commercially available and was used as received.

5-Mesityldipyrromethane,[18,19] 1,19-dideoxy-8,12-diethyl-2,3,7,13,17,18-hexamethyl-biladien-a,c,[20−22] 5-(13,17-diethyl-2,3,7,8,12,-

(5) Roszak, A. W.; Howard, T. D.; Southall, J.; Gardiner, A. T.; Law, C. J.; Isaacs, N. W.; Cogdell, R. J. *Science* **2003**, *302*, 1969.
(6) Savage, H.; Cyrklaff, M.; Montoya, G.; Kühlbrandt, W.; Sinning, I. *Structure* **1996**, *4*, 243.
(7) Walz, T.; Jamieson, S. J.; Bowers, C. M.; Bullough, P. A.; Hunter, C. N. *J. Mol. Biol.* **1998**, *282*, 833.
(8) Fleming, G. R.; Scholes, G. D. *Nature* **2004**, *431*, 256.
(9) Hu, X.; Ritz, T.; Damjanovic, A.; Schulten, K. *J. Phys. Chem. B.* **2003**, 76, 689.
(10) Takahashi, R.; Kobuke, Y. *J. Am. Chem. Soc.* **2003**, *124*, 2372.
(11) Faure, S.; Stern, C.; Guilard, R.; Harvey, P. D. *J. Am. Chem. Soc.* **2004**, *126*, 1253−1261.
(12) Förster, T. *Naturwissenschaften* **1946**, *33*, 166.
(13) Förster, T. *Ann. Phys.* **1948**, *2*, 55.
(14) Dexter, D. L. *J. Chem. Phys.* **1953**, *21*, 836.
(15) Faure, S.; Stern, C.; Espinosa, E.; Guilard, R.; Harvey, P. D. *Chem. Eur. J.* **2005**, *11*, 3469.
(16) A recent example for a sophisticated control of light harvesting process is found in Pascal, A. A.; Liu, Z.; Broess, K.; van Ort, B.; van Amerongen, H.; Wang, C.; Horton, P.; Robert, B.; Chang, W.; Ruban, A. *Nature* **2005**, *436*, 134.
(17) Strachan, J.-P.; Gentemann, S.; Seth, J.; Kalsbeck, W. A.; Lindsey, J. S.; Holten, D.; Bocian, D. F. *J. Am. Chem. Soc.* **1997**, *119*, 11191−11201.
(18) Lee, C.-H.; Lindsey, J. S. *Tetrahedron* **1994**, *50*, 11427−11440.
(19) Littler, B. J.; Miller, M. A.; Hung, C. H.; Wagner, R. W.; O'Shea, D. F.; Boyle, P. D.; Lindsey, J. S. *J. Org. Chem.* **1999**, *64*, 1391−1396.
(20) Barbe, J.-M.; Burdet, F.; Espinosa, E.; Gros, C. P.; Guilard, R. *J. Porphyrins Phthalocyanines* **2003**, *7*, 365−374.

Chart 2

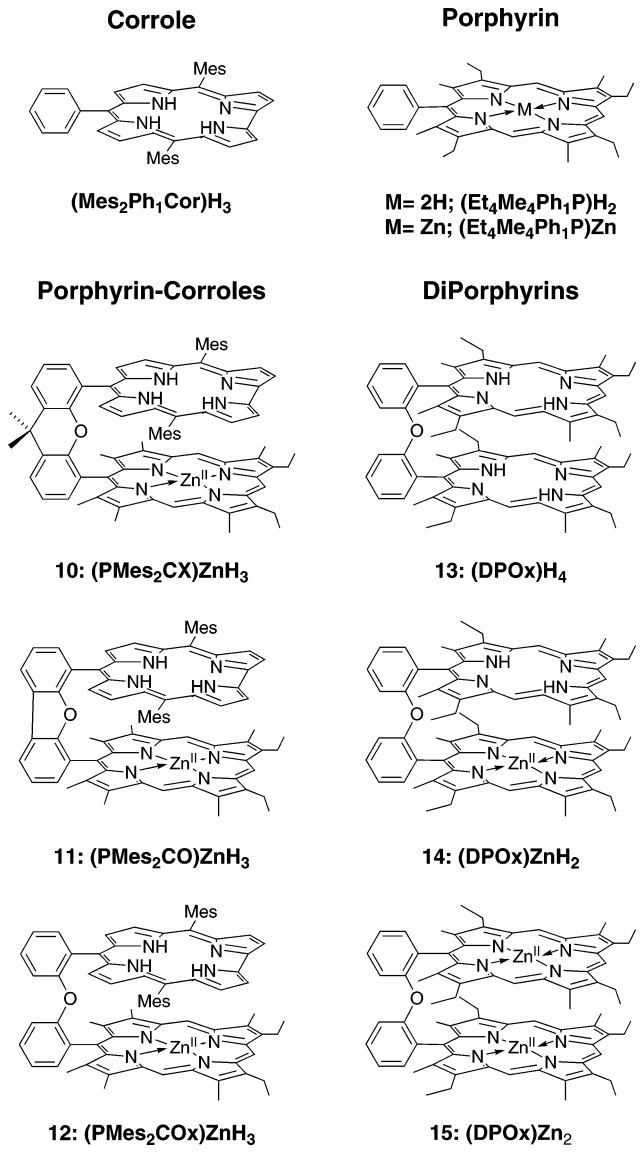

18-hexamethylporphyrin-5-yl)-4-formyl-dibenzofuran (**10**),[20,21] [5-[5-(5,15-dimesitylcorrol-10-yl)-9,9-dimethylxanthen-4-yl]-13,17-diethyl-2,3,7,8,12,18-hexamethylporphyrin]zinc[23] (**15**), and 2,2′-*bis*-(2,8,13,17-tetraethyl-3,7,12,18-tetramethylporphyrin-5-yl)diphenylether (DPOx)-H_4[24] (**16**) were synthesized as already described.

Synthesis and analytical data of 10-phenyl-5,15-dimesitylcorrole ($Mes_2Ph_1Cor)H_3$ (**6**), [5-[4-(5,15-dimesitylcorrol-10-yl)dibenzofuran]-13,17-diethyl-2,3,7,8,12,18-hexamethylporphyrin]zinc ($PMes_2$-CO)ZnH_3 (**14**), [5-[4-(5,15-dimesitylcorrol-10-yl)diphenylether]-13,17-diethyl-2,3,7,8,12,18-hexamethylporphyrin]zinc ($PMes_2COx$)-ZnH_3 (**13**), [2,2′-*bis*-(2,8,13,17-tetraethyl-3,7,12,18-tetramethylporphyrin-5-yl)diphenylether]Zn (DPOx)ZnH_2 (**17**), and [2,2′-*bis*-(2,8,-13,17-tetraethyl-3,7,12,18-tetramethylporphyrin-5-yl)diphenylether]-Zn_2 (DPOx)Zn_2 (**18**) are given in the Supporting Information (SI).

X-ray Crystallography. X-ray Diffraction Experiments and Data Processing for 17 and 18. Dark-red single-crystals of prismatic shape were grown from $CDCl_3$/MeOH (**17** and **18**). Specimens of very good crystal quality were selected for the X-ray diffraction experiments at $T = 115$ (2) K. The X-ray source was graphite-monochromatized Mo Kα radiation ($\lambda = 0.71073$ Å) from a sealed tube. Measurements were collected on a Nonius KappaCCD diffractometer,[25] equipped with a nitrogen jet stream low-temperature system (Oxford Cryosystems), up to $\theta_{max} = 27.5°$ for **17** and 30.0° for **18**. Lattice parameters were obtained by a least-squares fit to the optimized setting angles of 7388 (**17**) and 15142 (**18**) collected reflections in the theta ranges $1.0° < \theta < 27.5°$ and $1.0° < \theta < 30.0°$, respectively. Intensity data were recorded as φ- and ω-scans with κ offsets. No significant intensity decay was observed during the data collection. No diffractometer or temperature problems occurred during the experiments. Data reductions were done by using the DENZO software.[26]

Structure Solution and Refinement. The structures of **17** and **18** were solved in both *C*2 and *C*2/*c* space groups by direct methods using the SIR97 program.[27] In spite of the very nice results obtained with the *C*2/*c* space group, inspection of the *h*0*l*; $l = 2n + 1$ reflections clearly indicated that they were not systematic absences neither for **17** nor for **18**. Therefore, the *C*2 space group was selected for the crystal structure determinations and the *c* pseudo-symmetry glide plane element was not considered. In both cases, the best phase set in the solving procedure gave all the positions for the non-hydrogen atoms. Refinements were carried out by full-matrix least-squares on F^2 using the SHELXL97 program[28] and the complete set of reflections. Friedel pairs were not merged to estimate the Flack parameter. In the crystal structure of **17**, the metal center and the hydrogen atoms belonging to the pyrrolic nitrogens are disordered between both macrocyclic cavities, exhibiting sites occupation factors of 0.5/0.5. After the anisotropic thermal parameters refinement of the non-H atoms, all hydrogen atoms were located by Fourier synthesis, except those bonded to the pyrrole nitrogens (N_{pyr}) in **17** that were not found due to their structural disorder, coupled with that of the metal atom, between both macrocyclic cavities. Hydrogen atoms were refined with a global isotropic thermal factor using a riding model in both crystal structure determinations. At the convergence, the value of the Flack parameter was 0.52(2) and 0.50(1) for **17** and **18**, indicating that the pseudo-symmetry glide plane appearing in both crystal structure determinations can be associated either to a merohedral twin or to a racemic enantiomers mixture. Table 1 shows crystal data, as well as some experimental and refinement details.

Theoretical Computations. Calculations using the density functional theory (DFT) approximation were performed using the commercially available Gaussian 03 software.[29] The hybrid B3LYP exchange−correlation function has been considered due to the high accuracy of the ensued results,[30−32] with 3-21G* as the basis

(21) Kadish, K. M.; Ou, Z. P.; Shao, J.; Gros, C. P.; Barbe, J.-M.; Jérôme, F.; Bolze, F.; Burdet, F.; Guilard, R. *Inorg. Chem.* **2002**, *41*, 3990−4005.
(22) Guilard, R.; Jérôme, F.; Barbe, J.-M.; Gros, C. P.; Ou, Z.; Shao, J.; Fischer, J.; Weiss, R.; Kadish, K. M. *Inorg. Chem.* **2001**, *40*, 4856−4865.
(23) Barbe, J.-M.; Burdet, F.; Espinosa, E.; Guilard, R. *Eur. J. Inorg. Chem.* **2005**, 1032−1041.
(24) Tanaka, M.; Ohkubo, K.; Gros, C. P.; Guilard, R.; Fukuzumi, S. *J. Am. Chem. Soc.* **2006**, *128*, 14625−14633.
(25) *Nonius COLLECT, Data Collection Software*; Nonius, B. V.: Delft, The Netherlands, 1998.
(26) Otwinowski, Z.; Minor, W. *Methods Enzymol.* **1997**, *276*, 307−326.
(27) Altomare, A.; Burla, M. C.; Camalli, M.; Cascarano, G. L.; Giacovazzo, C.; Guagliardi, A.; Moliterni, A. G. G.; Polidori, G.; Spagna, R. *J. Appl. Crystallogr.* **1999**, *32*, 115−119.
(28) Sheldrick, G. M. *SHELXL97 Program for the Refinement of Crystal Structures*; University of Göttingen: Göttingen, Germany, 1997.
(29) Frisch, M. J. et al. *Gaussian 03, Revision C.02*; Gaussian, Inc.: Wallingford CT, 2004.
(30) Becke, A. D. *J. Chem. Phys.* **1993**, *98*, 5648−5652.
(31) Lee, C.; Yang, W.; Parr, R. G. *Phys. Rev. B: Condens. Matter Mater. Phys.* **1988**, 785−789.
(32) Miehlich, B.; Savin, A.; Stoll, H.; Preuss, H. *Chem. Phys. Lett.* **1989**, *157*, 200−206.

Table 1. Crystallographic Data for $(DPOx)ZnH_2$ (**17**) and $(DPOx)Zn_2$ (**18**)

compound	$(DPOx)ZnH_2$(**17**)	$(DPOx)Zn_2$ (**18**)
chemical formula	$C_{76}H_{80}N_8O_1Zn_1$	$C_{76}H_{78}N_8O_1Zn_2$
fw	1186.85	1250.2
temp, K	115(2)	115(2)
wavelength, Å	0.71069	0.71069
cryst syst	monoclinic	monoclinic
space group	*C*2	*C*2
a, Å	24.8280(3)	24.8884(2)
b, Å	14.9492(2)	14.9206(2)
c, Å	20.3763(2)	20.5194(2)
α, °	90	90
β, °	124.285(1)	125.443(1)
γ, °	90	90
V, Å^3	6248.76(15)	6207.85(13)
Z	4	4
μ, mm^{-1}	1.262	0.827
cryst size, mm^3	0.50 × 0.45 × 0.20	0.30 × 0.25 × 0.20
collected reflns	14 254	28 746
unique reflns	7388	16 842
R_{int}	0.0258	0.0211
θ_{max}, °	27.46	30.02
refinement method	full-matrix least-squares on F^2	full-matrix least-squares on F^2
GOF on F^2	1.063	1.017
R1/wR2[a] ($I > 2\sigma(I)$)	0.0496/0.1164	0.0338/0.0794
R1/wR2[a] (all data)	0.0673/0.1251	0.0486/0.0868
$\Delta\rho_{max}/\Delta\rho_{min}$, eÅ^{-3}	0.500/−0.265	0.370/−0.419

[a] $R1 = \Sigma||F_o| - |F_c||/\Sigma |F_o|$ and $wR2 = [\Sigma[w(F_o^2 - F_c^2)^2] / \Sigma [w(F_o^2)^2]]^{1/2}$.

set.[33−35] All computations were performed without symmetry constraint. The studied molecules were treated as bismetallated systems (i.e., Zn_2) to ensure that the macrocycles are rigid preventing various orientations of the pyrrole rings (NH pointing up and down). Clearly, zinc corroles are usually unstable[36] and were investigated only for geometry optimization purposes, keeping the macrocycle rigid.

Results and Discussion

10-Phenyl-5,15-dimesitylcorrole (**6**) was prepared following the one-pot synthesis of *trans*-A_2B-corroles already described in the litterature.[37] The condensation of 1 equiv of benzaldehyde on 2 equiv of mesityldipyrromethane[18,19] in the presence of catalytic amount of trifluoroacetic acid (TFA) in dichloromethane led to **6** in 5% yield (Scheme 1).

The synthesis of the three alkyl-porphyrin-*meso*-substituted-corroles was carried out following a procedure recently described in the literature by our group.[23] The synthesis requires the preparation of a key (porphyrin-aldehyde)zinc intermediate (e.g., **9** or **10**; Scheme 2).

The latter was prepared in >50% yield by acid-catalyzed condensation of 1 equiv of the corresponding a,c-biladiene to 1 equiv of the corresponding 1,8-diformyl derivatives (Scheme 2). The cyclization reactions were carried out starting from the zinc complexes of the (porphyrin-spacer-monoaldehyde) systems as the metalated porphyrins are easier to purify than the free-base analogs. 5-Mesityldipyrromethane[18,19] was used in twice the stoichiometric amount

Scheme 1. Synthesis of Free-Base Corrole **6**.

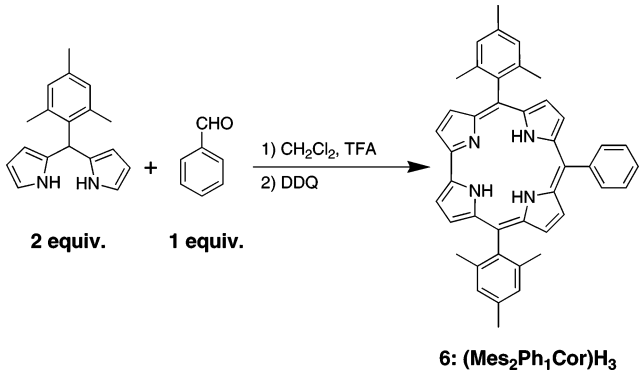

in the presence of a catalytic amount of TFA to provide in one step the desired cofacial porphyrin-corroles (**13**, **14**, or **15**; Scheme 2) in 34−35% yields. Corrole ring formation is easily evidenced by mass spectrometry (MALDI/TOF) by the presence of the molecular peak observed, in each case, as the most intense peak.

UV−visible spectral data of the cofacial porphyrin-corroles are summarized in Table 2, which also includes data for the related monocorrole (**6**) and monoporphyrin (**8**) having a similar substitution pattern. The Soret and Q bands for the three cofacial porphyrin-corroles are all blue-shifted compared to the spectrum of the related monocorrole (**6**, λ_{max} = 407, 425, 567, 604, and 637 nm) or the related monoporphyrin (**8**, λ_{max} = 410, 540, and 576 nm).[11] The UV−visible absorption spectra of the porphyrin-corroles are not just a simple arithmetic addition of the monocorrole and monoporphyrin spectra (Figures 1 and 2, and Supporting Information). They are slightly different, witnessing the presence of electronic interactions between the two macrocycles; a phenomenom previously reported for other Pacman porphyrins.[38−41] One interesting feature is that the *etio*-porphyrin/*etio*-porphyrin interactions induce a larger increase in bandwidth of the Soret band such as in **17** in comparison with the *etio*-porphyrin/$(Mes)_2$corrole ones, suggesting that the mesityl groups sterically prevent one macrocycle to fully interact with the other. This behavior is confirmed from the measurements of the singlet energy transfer rates and geometry optimizations below.

The flexible diphenylether diporphyrin **16** was prepared as previously described[24] via the classical three-branch synthesis described for the synthesis of analog cofacial pillared diporphyrins.[39,42−45] The mono- and dizinc deriva-

(33) Dobbs, K. D.; Hehre, W. J. *J. Comput. Chem.* **1986**, *7*, 359−378.
(34) Dobbs, K. D.; Hehre, W. J. *J. Comput. Chem.* **1987**, 8, 861−879.
(35) Dobbs, K. D.; Hehre, W. J. *J. Comput. Chem.* **1987**, *8*, 880−893.
(36) Paolesse, R.; Licoccia, S.; Boschi, T. *Inorg. Chim. Acta* **1990**, *178*, 9−12.
(37) Gryko, D.; Koszarna, B. *Synthesis* **2004**, *13*, 2205−2209.
(38) Bolze, F.; Drouin, M.; Harvey, P. D.; Gros, C. P.; Guilard, R. *J. Porphyrins Phthalocyanines* **2003**, *7*, 474−483.
(39) Bolze, F.; Gros, C. P.; Drouin, M.; Espinosa, E.; Harvey, P. D.; Guilard, R. *J. Organomet. Chem.* **2002**, *643−644*, 89−97.
(40) Bolze, F.; Gros, C. P.; Harvey, P. D.; Guilard, R. *J. Porphyrins Phthalocyanines* **2001**, *5*, 569−574.
(41) Harvey, P. D.; Proulx, N.; Martin, G.; Drouin, M.; Nurco, D. J.; Smith, K. M.; Bolze, F.; Gros, C. P.; Guilard, R. *Inorg. Chem.* **2001**, *40*, 4134−4142.
(42) Chang, C. J.; Deng, Y.; Heyduk, A. F.; Chang, C. K.; Nocera, D. G. *Inorg. Chem.* **2000**, *39*, 959−966.
(43) Collman, J. P.; Hutchison, J. E.; Lopez, M. A.; Tabard, A.; Guilard, R.; Seok, W. K.; Ibers, J. A.; L'Her, M. *J. Am. Chem. Soc.* **1992**, *114*, 9869−9877.
(44) Deng, Y.; Chang, C. J.; Nocera, D. G. *J. Am. Chem. Soc.* **2000**, *122*, 410−411.

Scheme 2. Synthesis of Monozinc Porphyrin-Corrole Dyads **13** and **14**.

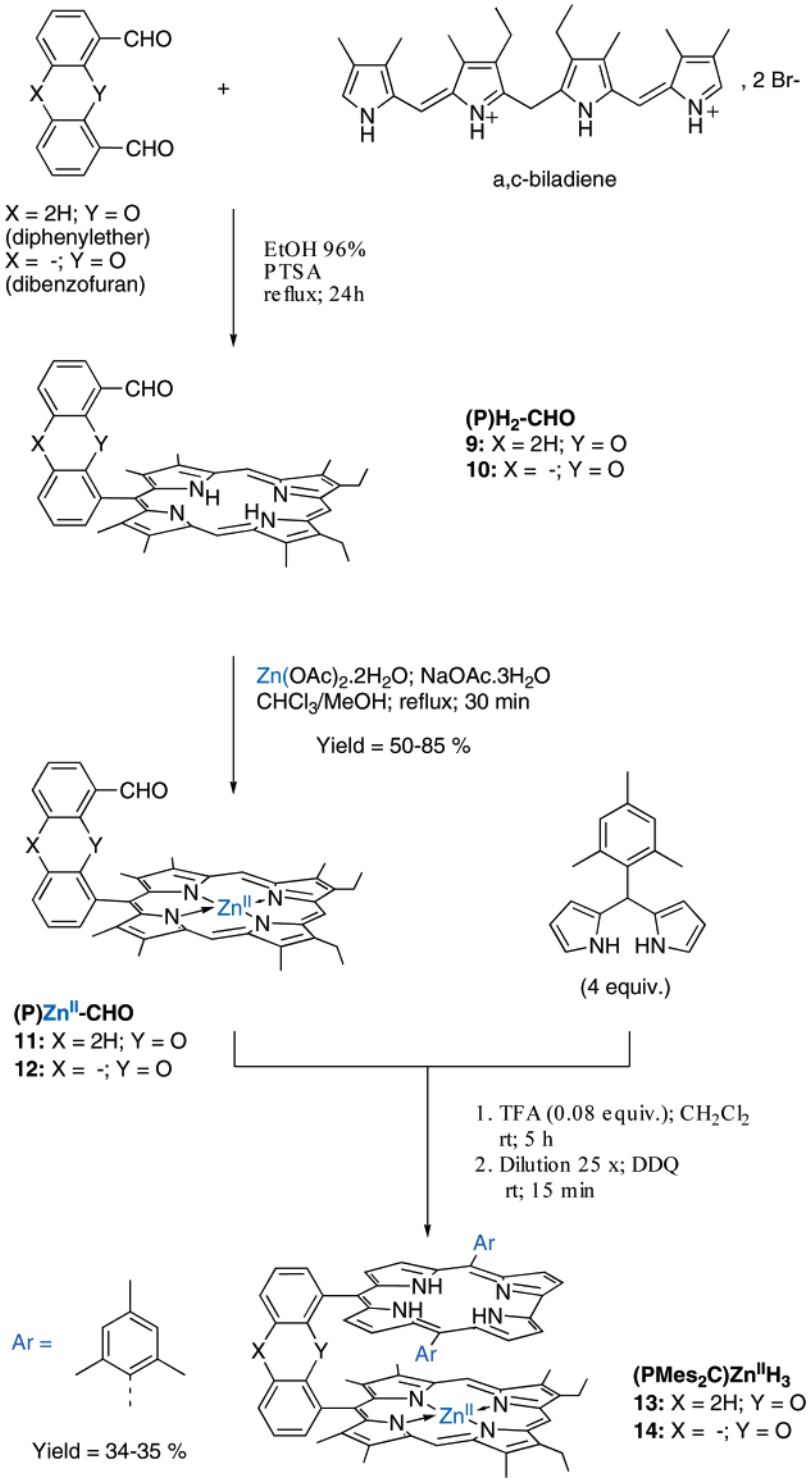

tives, respectively, **17** and **18**, were prepared following standard conditions as described in Scheme 3.[45,46]

The monitoring of the metalation reactions was performed by UV−visible spectroscopy and mass spectrometry (MALDI/TOF). The cofacial structures of the mono- and dizinc derivatives have been further confirmed by X-ray crystallography.

X-ray Crystallography. Compounds **17** and **18** crystallize in the monoclinic system (space group *C*2) with four molecular units per unit cell. In both cases, two halves molecular units form the asymmetric unit. Their crystal structures are isostructural, exhibiting very similar unit cell parameters and a relative unit cell volume difference less

(45) Tremblay-Morin J.-P.; Faure S.; Samar D.; Stern C.; Guilard R.; P., H. *Inorg. Chem.* **2005**, *44*, 2836−2842.
(46) Guilard, R.; Brandès, S.; Tardieux, C.; Tabard, A.; L'Her, M.; Miry, C.; Gouerec, P.; Knop, Y.; Collman, J. P. *J. Am. Chem. Soc.* **1995**, *117*, 11721−11729.

Table 2. Selected Absorption Maxima (ϵ, CH_2Cl_2) of Porphyrin-Corrole and Diporphyrin Dyads

		λ_{max}, nm ($\epsilon \times 10^{-4}$ mol^{-1} L cm^{-1})							
compound		Soret band		Q bands					ref[a]
$(Mes_2Ph_1Cor)H_3$	**6**	407 (11.7)	425 (8.9)	–	–	567 (1.7)	604 (1.2)	637 (0.6)	tw
$(Et_4Me_4Ph_1P)Zn$	**8**	410 (27)		–	540 (18)	576 (11)	–	–	11
$(PMes_2COx)ZnH_3$	**13**	403 (35.9)		–	536 (2.3)	570 (2.9)	–	–	tw
$(PMes_2CO)ZnH_3$	**14**	401 (50.4)		–	536 (2.9)	570 (4.0)	–	–	tw
$(PMes_2CX)ZnH_3$	**15**	399 (25.2)		–	540 (1.5)	574 (1.8)	–	–	22
$(DPOx)H_4$	**16**	391 (58.9)		506 (5.5)	540 (3.1)	574 (3.0)	–	627 (1.3)	23
$(DPOx)ZnH_2$	**17**	392 (31.9)		507 (1.0)	537 (1.9)	574 (1.9)	–	628 (0.1)	tw
$(DPOx)Zn_2$	**18**	392 (40.0)		–	538 (2.5)	574 (2.4)	–	–	tw

[a] tw = this work

than 1% (the unit cell volume observed for **17** is greater than that of **18** by ~40 Å^3). In **17**, the metal center and the hydrogen atoms belonging to the pyrrolic nitrogens are disordered between both macrocyclic cavities, exhibiting site occupation factors of 0.5/0.5. The observed disorder leads to a molecular structure that is extremely similar to that observed for **18**. Figure 3 shows the molecular view of **18**, which therefore can be also regarded as an almost equivalent structural representation of **17**, considering a 50% occupation of Zn at both metal atom positions and the corresponding 50% occupation of both H–(N_{pyr}) hydrogen atoms in the two macrocyclic cavities. Tables 3 and 4 show coordination bond distances and angles, along with main geometrical parameters of the cofacial bisporphyrins for both compounds, indicating only small structural differences between them.

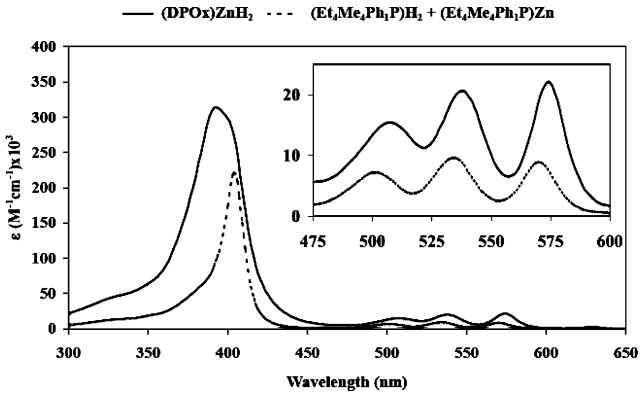

Figure 1. UV–vis spectra of $(Et_4Me_4Ph_1P)Zn$ (**8**) + $(Et_4Me_4Ph_1P)H_2$ (**7**) as compared to the monozinc derivative bisporphyrin $(DPOx)ZnH_2$ (**17**).

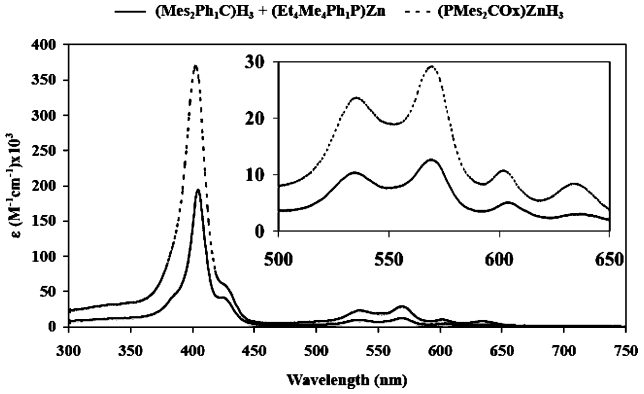

Figure 2. UV–vis spectra of $(Mes_2Ph_1Cor)H_3$ (**6**) + $(Et_4Me_4Ph_1P)Zn$ (**8**) as compared to the monozinc derivative porphyrin-corrole $(PMes_2COx)ZnH_3$ (**13**).

Unlike the dibenzofuran spacer, the diphenylether linker unit is more flexible. Thus, the intramolecular metal–metal distance is found shorter in **18** (6.12 Å) than in the dibenzofuran bisporphyrin complexes $(DPO)Zn_2$(2-ampyr),[47] $(DPO)Zn_2 \cdot MeOH \cdot CH_2Cl_2$,[44] $(DPO)Co_2 \cdot 2MeOH \cdot CH_2Cl_2$,[48] and $(DPO)Pd_2$[49] (6.68, 7.77, 8.62, and 6.81 Å, respectively). However, in spite of the spacer flexibility, the shortest metal–metal site distance in **17** and in **18** is found to be intermolecular (4.66 and 4.57 Å, respectively; Table 4), indicating that important intermolecular interactions are taking place in their crystal structures. As shown in the apical and in the molecular stacking views, (Figures 3 and 4), these interactions involve (i) the aromatic center of a pyrrolic group and a metal atom that is coordinated by the macrocyclic unit belonging to the closest bisporphyrin complex and (ii) $\pi-\pi$ interactions between the corresponding macrocyclic units. The coordination polyhedron of each metal center can be described as an elongated square bipyramid with the former aromatic center occupying one of the axial positions and a β-pyrrolic carbon atom belonging to the same bismacrocyclic unit placed on the other one (see Table 4).

Fluorescence Spectra. The fluorescence spectra and data for the investigated macrocycles are provided in Table 5 and Figure 5 (and the Supporting Information). While the homobismacrocycles exhibit typical spectra associated with the **8** zinc porphyrin[11] and **6** free-base corrole[50–52] chromophores, the dyads exhibit mostly the fluorescence associated with the acceptor. The fluorescence quantum yields (Table 6) compare favorably with those from the literature.[51] Presence of donor fluorescence is barely perceptible, providing evidence for singlet–singlet energy transfer processes. At 77 K, the **8** chromophore exhibits a phosphorescence where the 0–0 is observed at about 700 nm. This emission was not investigated in this work.

Energy Transfer. The through-space singlet–singlet energy transfers in cofacial dyads operate as described in Scheme 4.

(47) Chang, C. J.; Loh, Z.-H.; Deng, Y.; Nocera, D. G. *Inorg. Chem.* **2003**, *42*, 8262–8269.
(48) Chang, C. J.; Deng, Y.; Shi, C.; Chang, C. K.; Anson, F. C.; Nocera, D. G. *Chem. Commun. (Cambridge)* **2000**, 1355–1356.
(49) Loh, Z.-H.; Miller, S. E.; Chang, C. J.; Carpenter, S. D.; Nocera, D. G. *J. Phys. Chem. A* **2002**, *106*, 11700–11708.
(50) Ding, T.; Aleman, E. A.; Modarelli, D. A.; Ziegler, C. J. *J. Phys. Chem. A* **2005**, *109*, 7411–7417.
(51) Paolesse, R.; Sagone, F.; Macagnano, A.; Boschi, T.; Prodi, L.; Montalti, M.; Zaccheroni, N.; Bolletta, F.; Smith, K. M. *J. Porphyrins Phthalocyanines* **1999**, 364–370.
(52) Ventura, B.; Esposti, A. D.; Koszarna, B.; Gryko, D. T.; Flamigni, L. *New J. Chem.* **2005**, *29*, 1559–1566.

Scheme 3. Synthesis of Mono- and Dizinc Bisporphyrin Dyads (**17**) and (**18**).

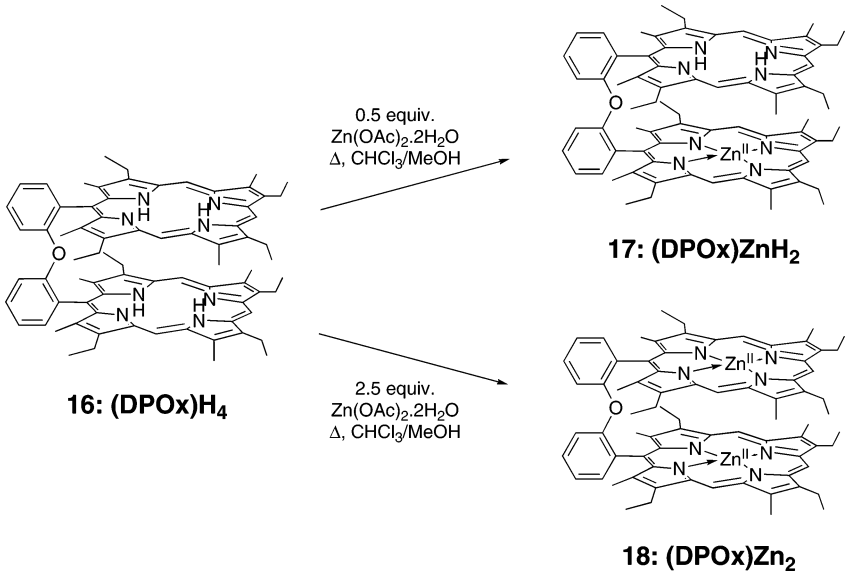

The rates for through-space energy transfer, k_{ET}, in **13**, **14**, **15**, and **17** can be evaluated by nano- and picosecond fluorescence lifetime of quantum yield measurements of the zinc porphyrin donor chromophore. Because of the difficulty in measuring the fluorescence quantum yield of the donor (due to extremely low intensity and inaccuracy in extracting the absorbance of the zinc porphyrin component in the absorption spectrum), the measurements of the fluorescence lifetimes were performed only. Using eq 1, one can evaluate k_{ET}:[53]

$$k_{ET} = (1/\tau_F) - (1/\tau_F^0) \quad (1)$$

τ_F is the fluorescence lifetime of the donor in the dyad, and τ_F^0 is the lifetime for a closely related bismacrocycle (when possible) where no energy transfer occurs. For example for **17**, **18** was employed as the standard. For the dissymmetric dyads **13**, **14**, and **15**, no bismacrocycle is totally appropriate

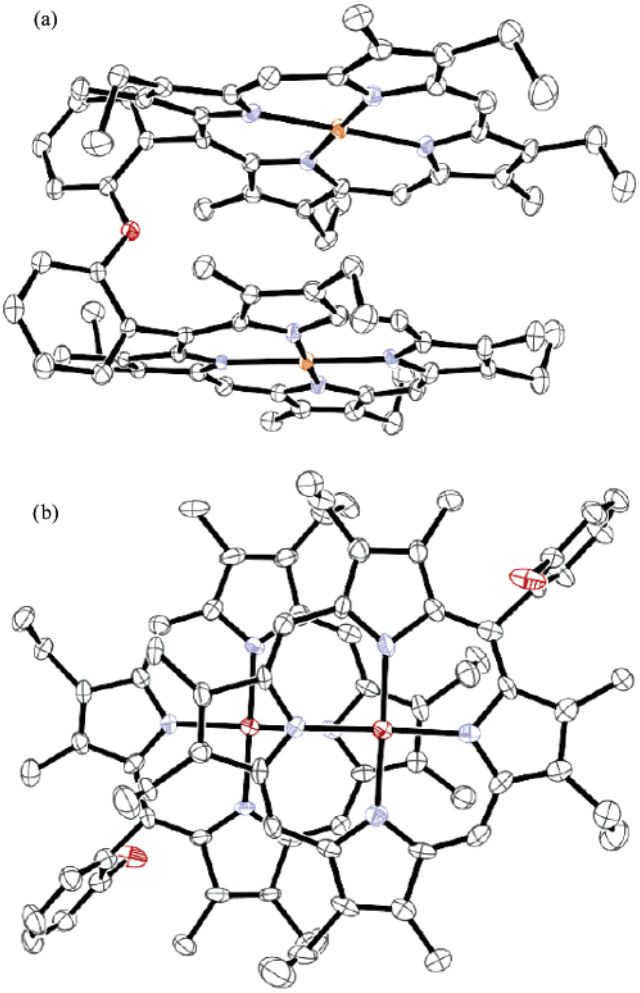

Figure 3. ORTEP view of homobimetallic (DPOx)Zn_2 (**18**) complex (thermal ellipsoids set at 50% probability level). (a) Molecular unit of the homobimetallic bisporphyrin complex (lateral view). (b) Two halves molecular units belonging to the asymmetric unit (apical view), showing the apical positions of the pyrrole groups in the intermolecular pyrrole−metal contacts. Hydrogen atoms are not represented for clarity.

Table 3. Selected Bond Distances (Å) and Angles (deg) for (DPOx)ZnH_2 (**17**)[a] and (DPOx)Zn_2 (**18**)

(DPOx)ZnH_2 (**17**)		(DPOx)Zn_2 (**18**)	
Zn(1A)−N(1A)	2.035(4)	Zn(1A)−N(1A)	2.001(5)
Zn(1A)−N(4A)	2.038(4)	Zn(1A)−N(3A)	2.037(5)
Zn(1A)−N(2A)	2.052(4)	Zn(1A)−N(4A)	2.047(4)
Zn(1A)−N(3A)	2.061(4)	Zn(1A)−N(2A)	2.051(4)
Zn(1B)−N(4B)	1.982(4)	Zn(1B)−N(1B)	2.031(4)
Zn(1B)−N(2B)	2.039(4)	Zn(1B)−N(2B)	2.040(4)
Zn(1B)−N(1B)	2.069(3)	Zn(1B)−N(3B)	2.053(4)
Zn(1B)−N(3B)	2.110(3)	Zn(1B)−N(4B)	2.058(4)
N(1A)−Zn(1A)−N(4A)	88.44(16)	N(1A)−Zn(1A)−N(3A)	177.99(17)
N(1A)−Zn(1A)−N(2A)	91.59(16)	N(1A)−Zn(1A)−N(4A)	89.88(16)
N(4A)−Zn(1A)−N(2A)	176.58(16)	N(3A)−Zn(1A)−N(4A)	91.38(18)
N(1A)−Zn(1A)−N(3A)	177.58(15)	N(1A)−Zn(1A)−N(2A)	90.73(16)
N(4A)−Zn(1A)−N(3A)	93.08(16)	N(3A)−Zn(1A)−N(2A)	87.92(18)
N(2A)−Zn(1A)−N(3A)	86.77(16)	N(4A)−Zn(1A)−N(2A)	176.64(16)
N(4B)−Zn(1B)−N(2B)	179.16(16)	N(1B)−Zn(1B)−N(2B)	91.35(18)
N(4B)−Zn(1B)−N(1B)	88.11(15)	N(1B)−Zn(1B)−N(3B)	176.93(16)
N(2B)−Zn(1B)−N(1B)	92.01(15)	N(2B)−Zn(1B)−N(3B)	89.18(17)
N(4B)−Zn(1B)−N(3B)	93.31(15)	N(1B)−Zn(1B)−N(4B)	88.21(17)
N(2B)−Zn(1B)−N(3B)	86.54(15)	N(2B)−Zn(1B)−N(4B)	179.2(2)
N(1B)−Zn(1B)−N(3B)	177.13(15)	N(3B)−Zn(1B)−N(4B)	91.22(16)

[a] For **17**, the bond distances and angles involving Zn(1A) and Zn(1B) refer to the sites occupied by the disordered zinc atom.

(53) Harvey, P. D.; Stern, C.; Gros, C. P.; Guilard, R. *Coord. Chem. Rev.* **2006**, in press.

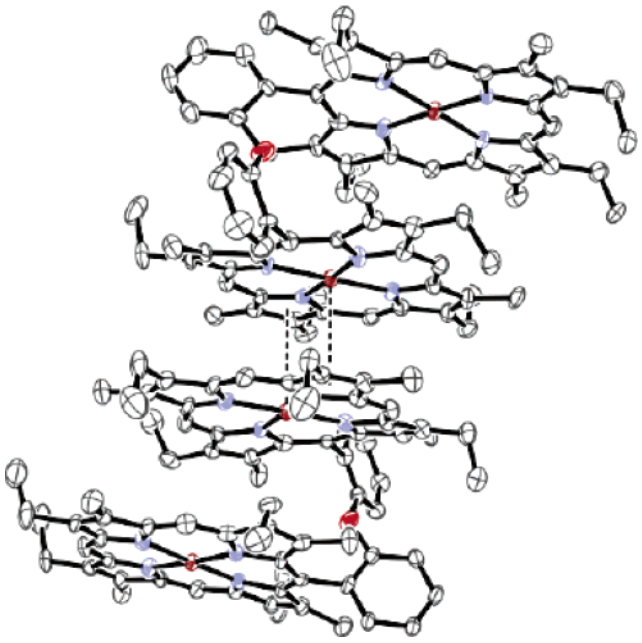

Figure 4. ORTEP view of the crystal packing of (DPOx)Zn_2 (**18**) (thermal ellipsoids set at 50% probability level) showing the Zn···pyrrole intermolecular interactions leading to short metal···π system distances along the [100] directions. Hydrogen atoms are not represented for clarity

since the dissymmetry leads intrinsically to a donor−acceptor system (therefore with an energy transfer process occurring no matter what).[54] For these cases, the standard was (Et_4-Me_4PhP)Zn in 2-MeTHF. The similarity in τ_F between this standard (1.70 and 1.94 ns at 298 and 77 K, respectively) and (DPO)Zn_2 (1.69 and 2.01 ns)[11] and (DPX)Zn_2 (1.73 and 1.94 ns),[11] two relevant bismacrocycles in this work, indicates that the uncertainty of this approximation is small. The data are compared in Table 5.

On the basis of these data, the observed rates for singlet−singlet through-space energy transfer for the new dyads are of the same order of magnitude as those published recently for the related compounds (**1**, **2**, **3**, **4**, and **5**). These rates are also slower than that for cofacial systems where photoinduced electron transfers were demonstrated.[53] On the basis of these comparisons, it is reasonably assumed that through space energy transfer is occurring in these new systems as well.

One trend is obvious, τ_F (at 298 and 77 K) for corrole-containing dyads are systematically larger than that for free-base porphyrin-containing dyads, indicating slower k_{ET}. This observation strongly suggests that one or both of the mesityl groups hinder the intermacrocycle interactions.

By replacing the rigid DPO spacer by the more flexible one, DPOx, singlet−singlet energy transfer still takes place as evidenced by a decrease in τ_F going from the standard molecule **18** to the dyads **17**. This result indicates that the cofacial conformation is still maintained in solution (since the linear conformation would lead to a much slower rate). This system also bares similarities with the flexible 1,2-ethanebis(octaethylporphyrin(zinc)); the latter was proven to

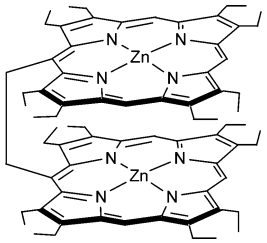

adopt a face-to-face geometry in solution.[55]

The larger k_{ET} value in the flexible system (**17**) ((DPOx)-ZnH_2 vs (DPO)ZnH_2 (**4**)) now suggests a better closing of the two macrocycles with respect to the more rigid DPO system. At 298 K, k_{ET} for **17** is similar to that of **2**, while at 77 K, this value resembles that found for **3**, showing, in overall, an effect similar to a decrease in donor−acceptor distances.

The ($PMes_2$COx)ZnH_3 dyad (**13**) is particularly interesting since it exhibits both features; the sterically demanding mesityl groups and flexible DPOx spacer, which have opposite effects on k_{ET}. While one can intuitively predict intermediate k_{ET} values between the faster **17** and slower **14** dyads, the experimental k_{ET} values are much closer to k_{ET} for **14** (and even slower at 77 K) and **15**. This comparison suggests intuitively that the steric effect has a more important effect on k_{ET} than the natural inter-macrocycle attractions via $\pi-\pi$ stacking. This is easy to understand with the perpendicularly placed steric mesityl group with respect to the donor macrocycle. All in all, the use of mesityl groups (here at the meso position) leads to the slower k_{ET}'s, notably at 77 K, which are the slowest in this family. Hence, k_{ET} can be modulated for a given spacer. Finally, because k_{ET} at 298 and 77 K for **15** and **13** are close to each other (Table 5), the cofacial nature of the latter dyads remains undoubtedly unchanged.

Geometry Optimization. In the absence of X-ray data for most of the investigated species, some useful information is extracted from geometry optimizations (DFT/B3LYP/3-21G*) in an attempt to corroborate the singlet−singlet energy transfer rates. The computational results are qualitative since the solvent−solute interactions are not taken into account notably for possible host−guest behavior. Such interactions are hard to anticipate. For comparison purposes, the geometry of "gas phase" (DPO)Zn_2 has been optimized as well (Figure 6) and exhibits the expected symmetric V-shaped structure. The slight differences with the available X-ray structure for the corresponding free base (DPO)H_4[39] are the orientation of some ethyl groups and a small inward deviation from perfect planarity of the porphyrin macrocycles (presumably due to a stacking effect). These have minor consequences in this study.

The comparison of the optimized geometry for (DPO)-Zn_2 and **18** is striking. **18** exhibits the expected cofacial

(54) The normal choice for a comparison standard would be a donor−donor bismacrocycle where no ET occurs but the intermacrocycle interactions for S_1 excited-state deactivation between 2-*etio*-porphyrin are different from that for *etio*-porphyrin···corrole(mesityl)$_2$. The bismacrocycle (Mes)$_2$biscorrole is not a good standard because the chromophore is an energy acceptor. Instead, compound **6** was used as the standard.

(55) Borovkov, V. V.; Lintuluoto, J. M.; Sugiura, M.; Inoue, Y.; Kuroda, R. *J. Am. Chem. Soc.* **2002**, 11282.

Table 4. Main Geometrical Parameters[a] of the Cofacial Bisporphyrins (DPOx)ZnH_2 (**17**)[b] and (DPOx)Zn_2 (**18**)

	(DPOx)ZnH_2 (**17**)	(DPOx)Zn_2 (**18**)
	Intramolecular	
$d_{intra(Zn\cdots Zn)}$	6.17 Å	6.12 Å
$d_{Zn2'\cdots Cpy2}$	3.62 Å	3.62 Å
$d_{Zn1\cdots Cpy8'}$	3.62 Å	3.62 Å
	Intermolecular	
$d_{inter(Zn\cdots Zn)}$	4.66 Å	4.57 Å
$d_{Zn1\cdots Ctpy6}$	3.36 Å	3.38 Å
$d_{Zn2\cdots Ctpy4}$	3.38 Å	3.39 Å
$\alpha_{Zn2'\text{-}Zn1\text{-}Zn2}$	167.4°	167.5°

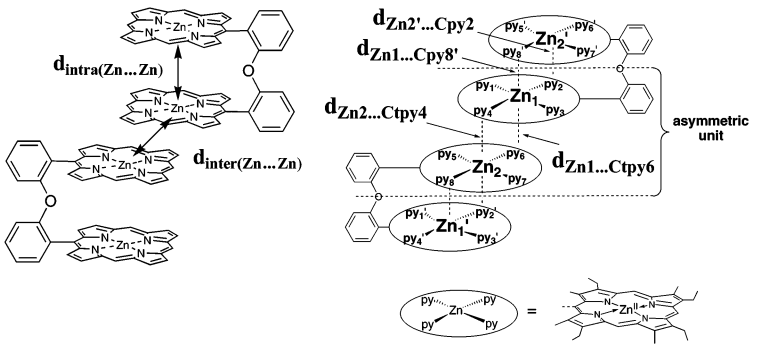

[a] While the intramolecular $d_{Zn\cdots Cpy}$ distances refer to the β-pyrrolic carbon atoms that are substituted by an ethylenic group, the intramolecular $d_{Zn\cdots Ctpy}$ distances refer to pyrrolic centroïds. The involved C_{py} atoms and Ct_{py} centroïds occupy the axial positions of the coordination sphere of Zn metal atoms, exhibiting one C_{py} atom and one Ct_{py} centroïd at each side of each metal center ($83.5 < \alpha(C_{py}-Zn-N_{py}) < 93.6°$ for Cpy_2 and Cpy_8' in both crystal structures, $88.5 < \alpha(Ct_{py6}'-Zn_1-N_{py}) < 93.6°$ and $88.4 < \alpha(Ct_{py4}'-Zn_2-N_{py}) < 93.0°$ for **18**, and $89.3 < \alpha(Ct_{py6}'-Zn_1-N_{py}) < 92.5°$ and $88.5 < \alpha(Ct_{py4}'-Zn_2-N_{py}) < 92.3°$ for **17**). [b] For **17**, the $d_{Zn\cdots Cpy}$ and $d_{Zn\cdots Ctpy}$ distances and the $\alpha_{Zn_2'-Zn_1-Zn_2}$ angle concern the sites occupied by the disordered zinc atom.

Table 5. Comparison of the τ_F and k_{ET} Data for **13**−**18**[a]

	τ_F (ns)		k_{ET} (ns^{-1})			
compound	298 K	77 K	298 K[b]	77 K[b]	donor standard	ref[a]
(Mes_2Ph_1Cor)H_3 (**6**)	6.8	9.0	−	−	−	tw
($Et_4Me_4Ph_1P$)Zn (**8**)	1.70	1.94	−	−	−	11
(DPB)Zn_2	0.63	1.80	−	−	−	11
(DPX)Zn_2	1.73	1.94	−	−	−	11
(DPO)Zn_2	1.69	2.01	−	−	−	11
(DPS)Zn_2	1.95	1.85	−	−	−	11
(DPB)ZnH_2 (**1**)	0.05	0.06	20.8	15.4	(DPB)Zn_2	11
(DPX)ZnH_2 (**2**)	0.10	0.09	9.8	10.9	(DPX)Zn_2	11
(DPA)ZnH_2 (**3**)	0.14	0.13	6.4	7.2	(Et_4Me_4PhP)Zn (**8**)	11
(DPO)ZnH_2 (**4**)	0.18	0.16	5.0	5.9	(DPO)Zn_2	11
(DPS)ZnH_2 (**5**)	0.19	0.19	4.7	4.6	(DPS)Zn_2	11
($PMes_2COx$)ZnH_3 (**13**)	0.46	1.10	1.6	0.3	(Et_4Me_4PhP)Zn (**8**)	tw
($PMes_2CO$)ZnH_3 (**14**)	0.40	0.80	3.1	6.8	(Et_4Me_4PhP)Zn (**8**)	tw
($PMes_2CX$)ZnH_3 (**15**)	0.57	0.80	1.2	0.7	(Et_4Me_4PhP)Zn (**8**)	tw
(DPOx)ZnH_2 (**17**)	<0.10	0.15	>9.4	6.7	(DPOx)Zn_2 (**18**)	tw
(DPOx)Zn_2 (**18**)	1.77	1.22	−	−	−	tw

[a] All in 2-MeTHF. [b] $1 \times (ns^{-1}) = 1 \times 10^9\ s^{-1}$. [c] tw = this work.

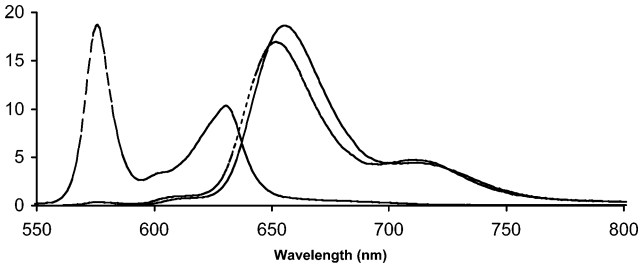

Figure 5. Fluorescence spectra of ($PMes_2CO$)ZnH_3 (**14**) (dotted), ($Et_4Me_4Ph_1P$)Zn (**8**) (dashed), and (Mes_2Ph_1Cor)H_3 (**6**) (bold) at 298 K in 2-MeTHF.

Table 6. Luminescence Data for the Mono and Bismacrocycles[a]

	quantum yields	λ_{max} (nm)	
compound	(298 K)[b]	298 K	77 K
(Mes_2Ph_1Cor)H_3 (**6**)	0.0718	655, 714	604, 645, 659, 706
(OEP)Zn	0.0217	576, 630	572, 628, 696
($PMes_2COx$)ZnH_3 (**13**)	0.0588	576, 648, 704	573, 603, 644, 659, 701
($PMes_2CO$)ZnH_3 (**14**)	0.0518	575, 651, 711	573, 602, 641, 658, 702
($PMes_2CX$)ZnH_3 (**15**)	0.0640	575, 654, 712	572, 610, 646, 668, 701
(DPOx)ZnH_2 (**17**)	0.0387	586, 631, 698	581, 625, 692
(DPOx)Zn_2 (**18**)	0.0177	586, 640	581, 635, 706, 790

[a] All in 2-MeTHF. [b] Uncertainty ±10%. The quantum yield is for all the fluorescence. For the dyads, the intensity of the donor fluorescence is weaker than the uncertainty.

geometry, but the V-shaped structure is not retained. Instead, the molecular scaffolding collapses and the two macrocycles lie close to each other in a parallel fashion, somewhat similar to that for (DPB)H_4 and (DPB)M_2 (M = Cu, Co) systems.[43,56] This contrasts with the reported X-ray structures for **17** and **18** in this work and is due to the easier intermolecular porphyrin−porphyrin interactions in the solid state. The intramolecular interactions are not surprising in the "gas phase" optimized geometry, since no intermolecular interactions are possible (Figure 6b). No intermolecular interactions are anticipated as well in diluted solution. This structure shows an obvious twisting of the $C_{meso}-Zn$ axes (47.7° instead of parallel). The flexible DPOx ligand allows closer intramolecular interactions. Some closest distances are $C_{meso}\cdots C_{meso} = 4.2$, $N\cdots N = 3.6$, and $C\cdots Zn = 3.2$ Å. These short distances are consistent with the observed faster rate

(56) Fillers, J. P.; Ravichandran, K. G.; Abdalmuhdi, I.; Tulinsky, A.; Chang, C. K. *J. Am. Chem. Soc.* **1986**, *108*, 417−424.

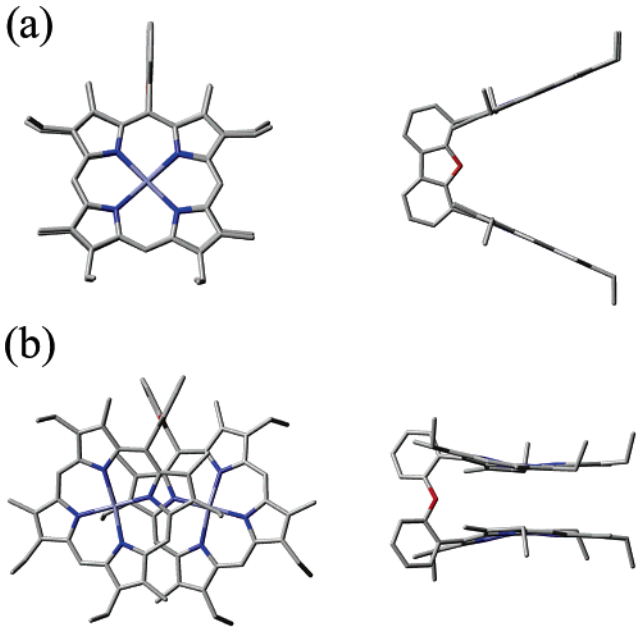

Figure 6. Top and side views of the optimized geometry for $(DPO)Zn_2$ (top) and $(DPOx)Zn_2$ (**18**) (bottom).

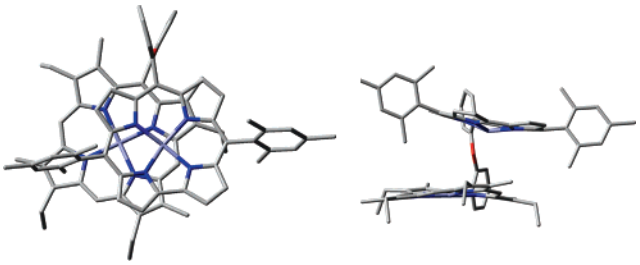

Figure 7. Top and side view of the optimized geometry for $(PMes_2COx)$-ZnH_3 (**13**).

Scheme 4. Representation of the Energy-Transfer Process.

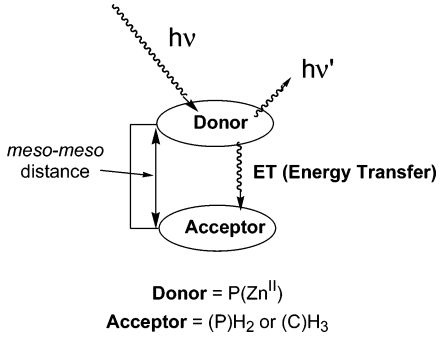

of **17** (>9.4 at 298 K and 4.7 ns^{-1} at 77 K) in comparison with **4** (5.0 at 298 K and 5.9 ns^{-1} at 77 K). One may wonder if the shortest distances in **17** are shorter than that found for $(DPB)ZnH_2$ why the rates are not faster. The answer lies in the probability of transfer. The geometry optimizations indicate the presence of twisting (47.7°; Scheme 5) allowing only a fraction of the porphyrin macrocycle to be in close proximity with the other (less than half).

As stated, the introduction of the $(Mes)_2$corrole free base as acceptor induces a systematic decrease in k_{ET} when comparing **4** vs **14**, **2** vs **15**, and **17** vs **13**.

The rates for **4** are 5.0 and 5.9 ns^{-1} at 298 and 77 K, respectively, faster than 3.1 and 4.8 ns^{-1}, respectively, for

Scheme 5. Drawing Showing the Area of the Porphyrin Macrocycles with Close Electronic Distances for Efficient ET in the "twisted" Dimer $(DPOx)ZnH_2$ (**17**) in Comparison with the Cofacial $(DPB)ZnH_2$ (**1**).

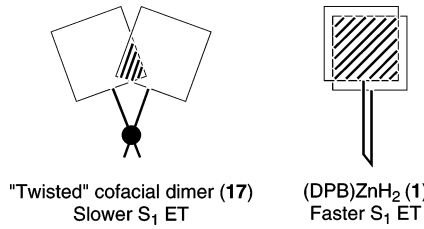

Scheme 6. Drawing Showing the Relative Orientations of the Macrocycles in Dyads $(DPO)ZnH_2$ (**4**) and $(PMes_2CO)ZnH_3$ (**14**).

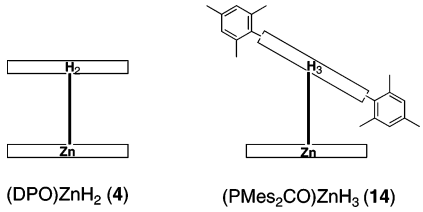

Scheme 7. Drawing of the Possible Fluxional Process at 298 K for $(PMes_2CO)ZnH_3$ (**14**).

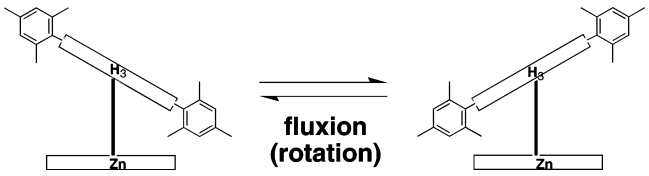

14. The 77 K data ($(DPO)ZnH_2$ which are faster than **14**), suggest overall closer distances between macrocycles. The geometry optimization for **14** (see Figure S1, SI) shows a rotated corrole pointing one mesityl group toward the porphyrin macrocycle, presumably due to hydrophobic interactions between the methyl residue with the π-system (Schemes 6 and 7). This rotation is possible because there is no methyl group at the β-positions.

However, while some interatomic distances increase, other decrease. Overall, "qualitatively" there is no substantial gain or loss in ET. Interestingly, the average rates ((298 + 77 K)/2) are 5.5 and 5.0 ns^{-1} for **4** vs **14**, respectively. A closer look at the 77 K case (where no intramolecular motion occurs) indicates that k_{ET} ($(PMes_2CO)ZnH_3$) > k_{ET} ($(DPO)ZnH_2$). This is entirely consistent with a Förster and Dexter mechanisms,[11−13] which states that k_{ET} is given by

$$k_{ET}^{\text{Förster}} = k_D R_F^6 \left(\frac{1}{r}\right)^6 \tag{2}$$

$$k_{ET}^{\text{Dexter}} = \frac{2\pi}{h} K J' \exp\left(\frac{-2r}{L}\right) \tag{3}$$

where k_D is the emission rate constant for the donor, R_F is the Förster radius, i.e., the distance at which transfer and spontaneous decay of excited donors are equally probable, r is the distance between the two macrocycles, J' is the integral overlap, K is an experimental constant, and L is the average Bohr radius (L = 4.8 for porphyrin).[53,56]

Because some atom−atom distances are short and others are long, one can consider the overall rate as the sum of all

Scheme 8. Drawing of $(PMes_2CX)ZnH_3$ (**15**) Showing the Slipping-Rotation Due to Steric Interactions of the Mesityl Fragments (left), and the Rotated Version (right).

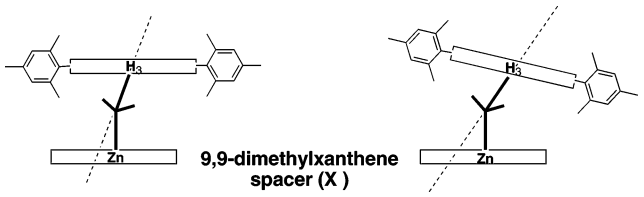

rates. Because the relationship is $(1/r)^6$ (Förster) and $\exp(-2r/L)$ (Dexter), the short distance interactions contribute significantly more than the longer ones. This explains the trend at 77 K where a frozen conformation exists.

At 298 K, the rate is now k_{ET} ($(PMes_2CO)ZnH_3$) < k_{ET} ($(DPO)ZnH_2$). Considering a weak activation energy to fluxion (as shown in Scheme 7), the average conformation is the donor and acceptor being parallel. It is proposed that the average conformation undergoes some steric interactions pushing away the two macrocycles from each other, explaining the slightly slower decrease at this temperature.

The comparison between **15** and **2** (k_{ET} ($(PMes_2CX)ZnH_3$) $\ll$ k_{ET} ($(DPX)ZnH_2$) suggests multiple factors contributing to the large decrease. From geometry optimization, three structural features are obvious (the X-ray data for $(DPX)H_4$ are available for comparison purposes).[57] There is a rotation about the $C_{spacer}-C_{meso}$(Cor) bond (Scheme 8). In addition, a small slipping is observed (see Figure S1a, SI), decreasing the number of short atom−atom distances for interactions.

Finally, the third observation is the obvious steric hindrance (mesityl-porphyrin) inducing macrocycle distortion, notably in the *etio*-type porphyrin chromophore, also contributing to the overall increase in atom−atom distances. The mesityl−mesityl axis is now bent in the optimized geometry. Similar conclusions can be drawn for **13** vs **17** (k_{ET} (**13**) $\ll$ k_{ET} (**17**)).[57] One last possible explanation about the observed slower rates in mesityl-containing dyads is suggested. On the basis of the geometry optimizations, clear mesityl···macrocycle contacts are obvious, where one of the mesityl group is placed almost between the donor and the acceptor chromophores. One may also wonder whether these groups or atoms interfere with the through-space process. To our knowledge, there is no other precedent for cofacial systems.

Conclusion

Experimental evidence is provided showing that through space singlet−singlet k_{ET} can be modulated via simple structural modifications, notably via steric hindrance and gain in spacer flexibility. With qualitative information extracted from the "gas phase" DFT geometry optimization, one can conclude that the relative orientation of the cofacial donor−acceptor dyads plays a key role on the k_{ET} values (twisted dimer and rotated chromophore), allowing one to modulate k_{ET}. Steric hindrance induces a decrease in k_{ET}, and a gain in spacer flexibility (in the absence of steric hindrance) increases k_{ET}.

However, the overall analysis of this work also brings a new light to the Förster and Dexter theories. Equation 3 relates the chromophore as a whole, while this work clearly demonstrates that the through-space ET depends on the relative orientation of the chromophores. Therefore, each atom involved in the frontier orbitals of the first macrocycle interacts individually with the atoms of the cofacial chromophore. Therefore, these theories could be better described as

$$\bar{k}_{ET}^{\text{Förster}} = k_D R_F^6 \sum_i \left(\frac{1}{r_i}\right)^6 \quad (4)$$

$$\bar{k}_{ET}^{\text{Dexter}} = \frac{2\pi}{h} KJ' \sum_i \exp\left(\frac{-2r_i}{L}\right) \quad (5)$$

where $\bar{k}_{ET}$ is an average rate and i is a given atom−atom interaction in the dyad. This improvement could bring a better understanding of through-space processes in general. This work also brought the suspicion that the presence of a group or an atom between the donor and acceptor part of the dyad involved in an ET process influences the rate. Future works on both above conclusions are in progress.

Acknowledgment. The Natural Sciences and Engineering Research Council of Canada (NSERC) and the Centre National de Recherche Scientifique (CNRS; UMR 5633) are acknowledged for funding.

Note Added after ASAP Publication. There were errors to a compound name and chemical formulas in Table 1 and there was an error in the Table 4 footnote in the version published ASAP December 10, 2006; the corrected version was published December 18, 2006.

Supporting Information Available: Instrumentation, synthetic procedures and analytical data of **6**, **14**, **13**, **17**, and **18**; X-ray crystallographic file (CIF) for **17** (CCDC-610234) and **18** (CCDC-610233); views of the optimized geometry for **15** and **14** (Figure S1); UV−vis spectra of bisporphyrins **16** (Figure S2) and **18** (Figure S3) and porphyrin-corroles **13**, **14**, and **15** (Figure S4); fluorescence spectra of **14** in 2-MeTHF at 77 K (Figure S5); and complete ref 29. This material is available free of charge via the Internet at http://pubs.acs.org.

IC0613558

(57) Chang, C. J.; Baker, E. A.; Pistorio, B. J.; Deng, Y.; Loh, Z.-H.; Miller, S. E.; Carpenter, S. D.; Nocera, D. G. *Inorg. Chem.* **2002**, *41*, 3102.